Supplementary Material

Evidence of Covid-19 lockdown effects on riverine dissolved organic matter dynamics provides a proof-of-concept for needed regulations of anthropogenic emissions

Retelletti Brogi S.[1], Cossarini G. [2], Bachi G. [1], Balestra C.[2], Camatti E.[1,3], Casotti R.[4], Checcucci G. [1], Colella S.[5], Evangelista V. [1], Falcini F.[5], Francocci F.[6], Giorgino T.[7], Margiotta F. [4], Ribera d'Alcalà M. [4], Sprovieri M.[8], Vestri S. [1], Santinelli C. [1]

[1] *Istituto di Biofisica, CNR. Pisa, Italy.*

[2] *Istituto Nazionale di Oceanografia e Geofisica Sperimentale. Sgonico (TS), Italy.*

[3] *Istituto di Scienze Marine, CNR. Venezia, Italy.*

[4] *Stazione Zoologica Anton Dohrn. Napoli, Italy.*

[5] *Istituto di Scienze Marine, CNR. Roma, Italy*

[6] *Istituto per lo studio degli impatti Antropici e Sostenibilità in ambiente marino, CNR. Roma, Italy.*

[7] *Istituto di Biofisica, CNR. Milano, Italy.*

[8] *Istituto per lo studio degli impatti Antropici e Sostenibilità in ambiente marino, CNR. Campobello di Mazara (TP), Italy.*

Figure S1. Results of the specsse test within drEEM showing the effect of the model when adding more components, expressed as the sum of squared error for each model. The plots show that the 6 component model is the one with the lower error in both excitation (upper panel) and emission (lower panel).

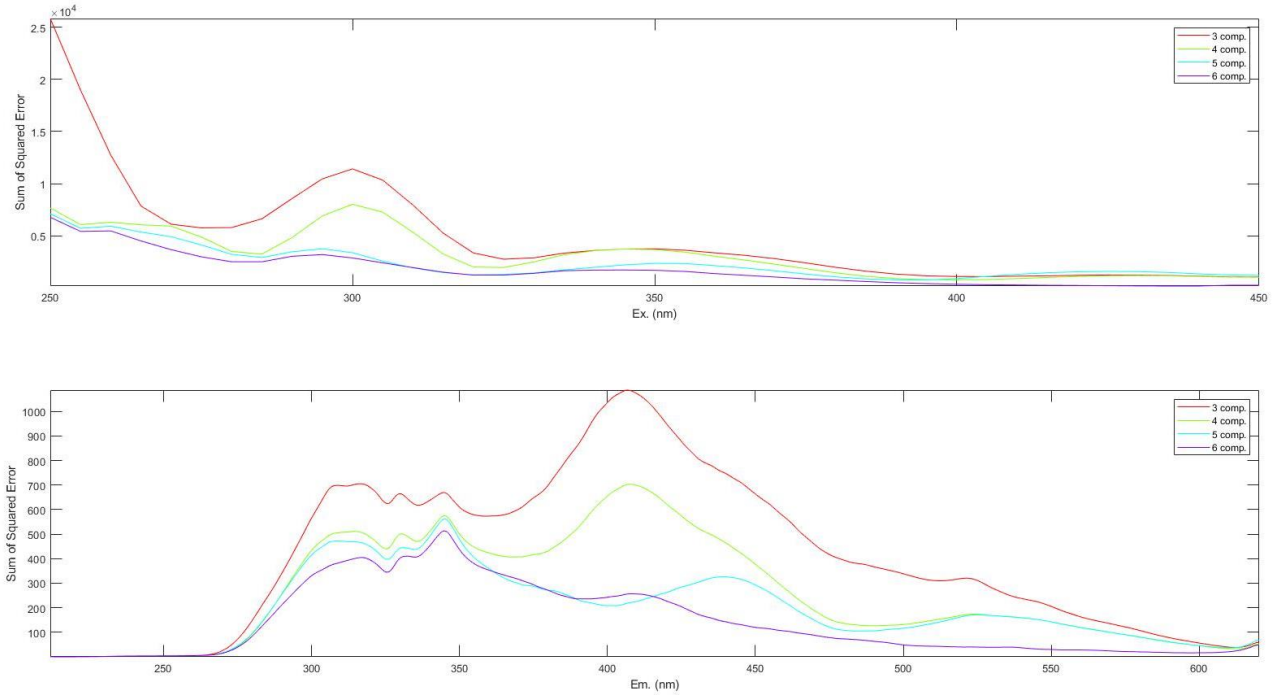

Figure S2. Example of inspection of the residuals for the validation of the PARAFAC model. Here we compare the 3 components model (upper panels) with the 6 components model (lower panels). The plots show the original sample on the left, the modeled one in the center, and the difference between the two on the right (i.e. the residuals)

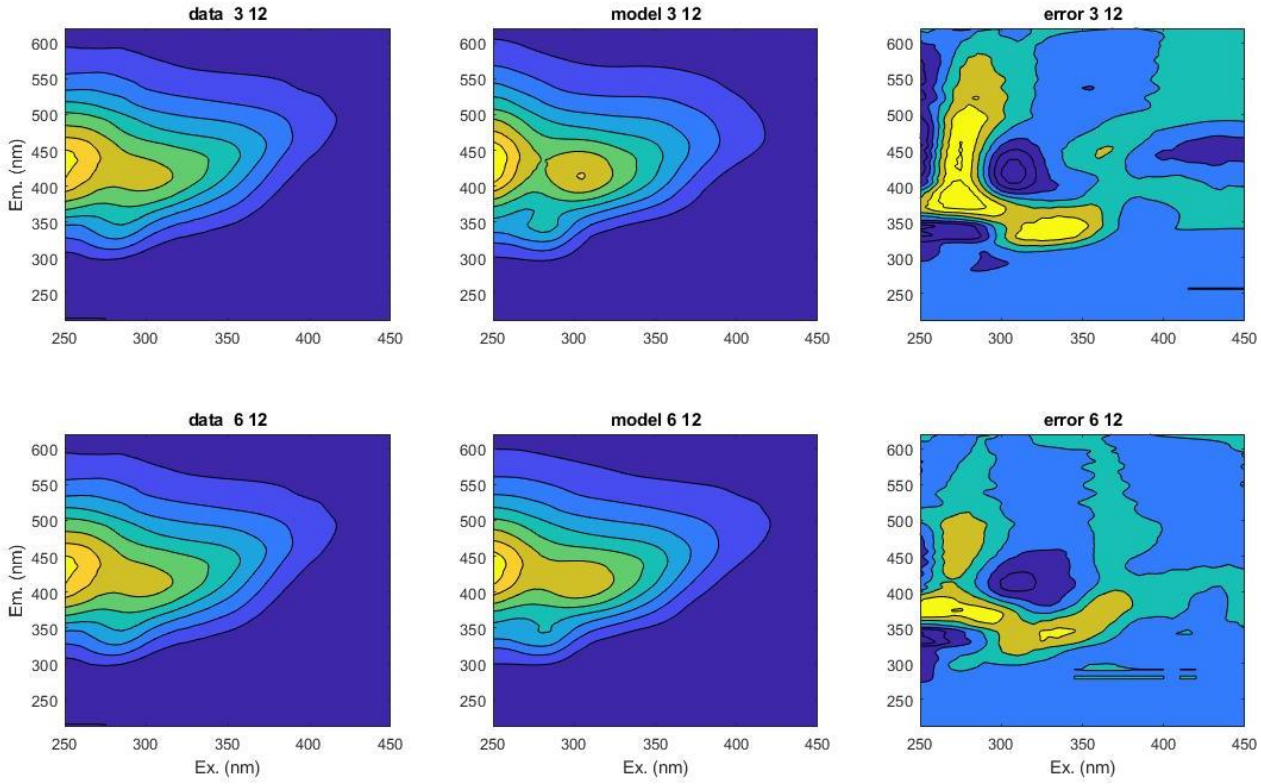

Figure S3. Core consistency results for the 6 components model.

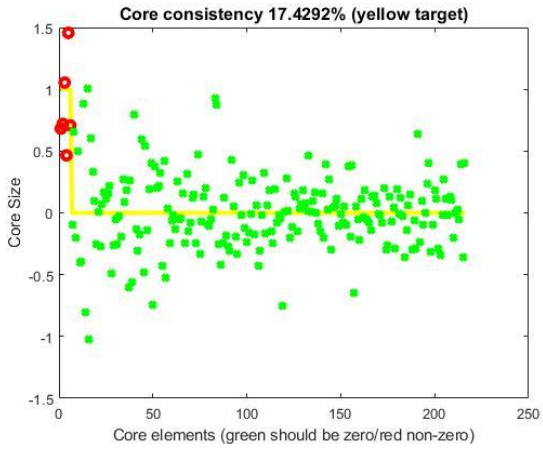

Figure S4. Results of the split validation tool within the drEEM

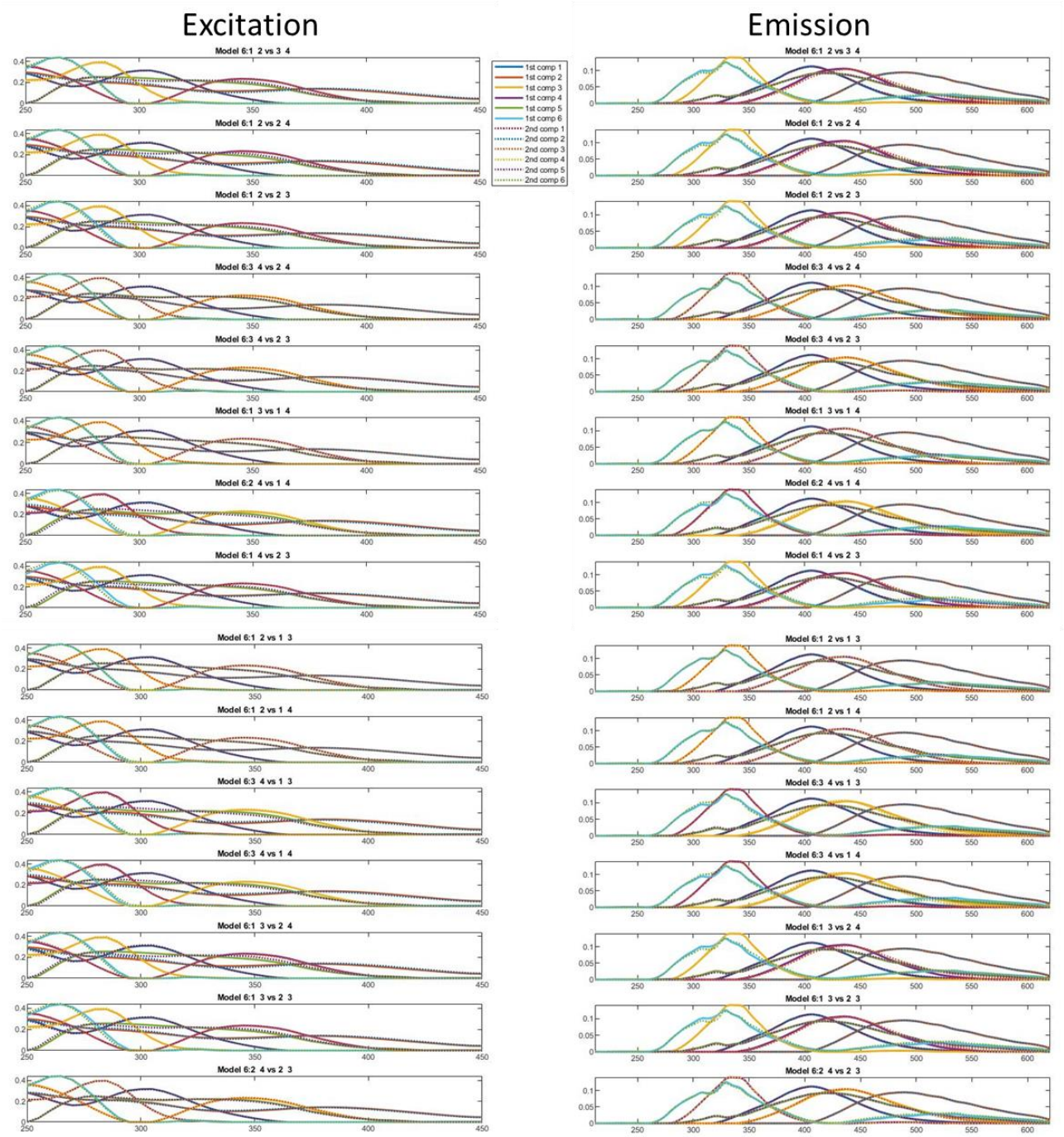

Figure S5. Results of the 6 components model validation carried out within the drEEM tool.

```
val6 =
  struct with fields:

                          Ex: [41×1 double]
                          Em: [500×1 double]
                           X: [468×500×41 double]
                IntensityUnit: 'RU'
                         nEx: 41
                         nEm: 500
                     nSample: 468
                          ID: {468×1 cell}
                   Xnotscaled: [468×500×41 double]
                   Preprocess: 'Normalised to unit variance in sample mode'
                        Split: [1×6 struct]
       Split_NumBeforeCombine: 4
                 Split_Style: 'alternating then combine'
        Split_NumAfterCombine: 6
           Split_Combinations: {'1  2'  '3  4'  '1  3'  '2  4'  '1  4'  '2  3'}
                Split_nSample: [234 234 234 234 234 234]
              Split_AnalRuns: [5 5 5 5 5 5]
     Split_PARAFAC_Initialise: 'Random'
        Split_PARAFAC_options: [1.0000e-06 2 0 0 0 0]
    Split_PARAFAC_constraints: [2 2 2]
      Split_PARAFAC_convgcrit: [1.0000e-06 1.0000e-06 1.0000e-06 1.0000e-06 1.0000e-06 1.0000e-06]
                      Model6: {3×1 cell}
               Val_ModelName: 'Model6'
              Val_Preprocess: 'Reversed normalisation to recover true scores'
                 Val_Source: 'Model6it_7'
                   Val_Err: 5.9662e+04
                    Val_It: 70
                  Val_Core: 17.4292
               Val_ConvgCrit: 1.0000e-06
             Val_Constraints: 'nonnegativity'
              Val_Initialise: 'random'
             Val_PercentExpl: 99.6152
                Val_CompSize: [48.0472 33.1062 30.8155 14.7680 21.0592 5.0615]
                 Val_Result: 'Overall Result= Validated for all comparisons'
             Val_Comparisons: {'AB vs CD,'  'AC vs BD,'  'AD vs BC,'}
         Val_Comparisons_Num: [3×2 double]
                Val_Matches: {4×1 cell}
                   Val_ExCC: {4×1 cell}
                   Val_EmCC: {4×1 cell}
                 Val_Splits: {'AB'  'CD'  'AC'  'BD'  'AD'  'BC'}
              Val_SplitsNum: [1 2 3 4 5 6]
```

Figure S6. Excitation (blue) and emission (red) spectra of the six components validated by the application of PARAFAC analysis to 533 EEMs (2020-2021 dataset plus the data from 2014-2015). The numbers indicate the wavelength of each spectrum peak.

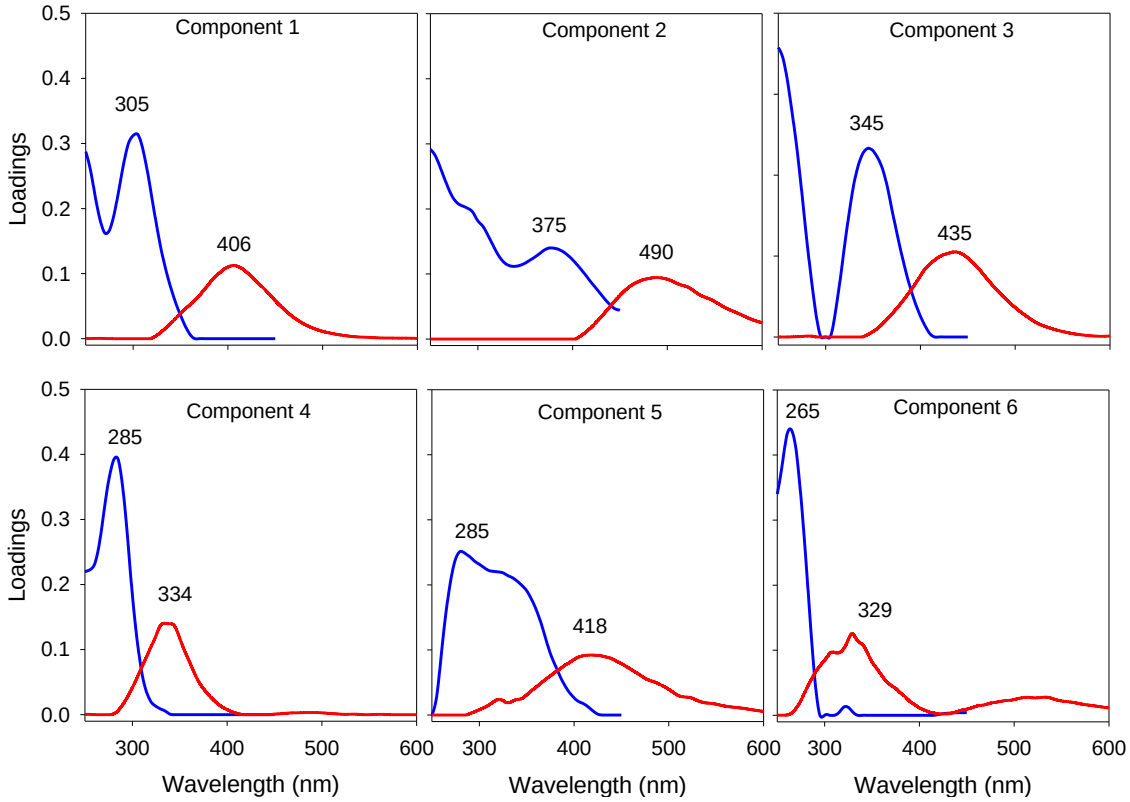

Figure S7. Contour plots of the components validated by PARAFAC.

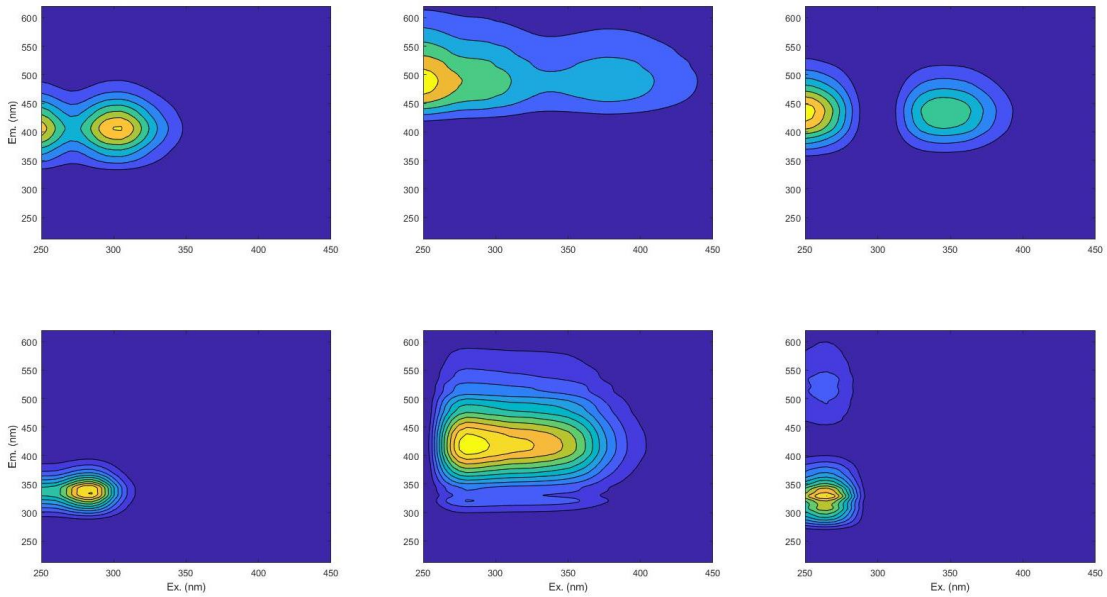

Table S1. Characteristics of the components, their characterization, and references to similar components found in the literature. The comparison with the components was done either by using the Openfluor database (Murphy et al., 2014b) or by comparing the excitation and emission maxima with published components not present in the database.

Components	λex peak (nm)	λem peak (nm)	Idetification	Similar components
C1	<250, 305	406	Microbial humic-like	**C1** Retelletti Brogi et al., 2020 **C5** Lapierre and Del Giorgio, 2014 **C2** Murphy et al., 2011 **C4** Meng et al., 2013 **C6** Maie et al., 2014 **C3** Lambert et al., 2016 **C1** Ferretto et al., 2017 **Peak β** Parlanti et al., 2000
C2	<250, 375	490	Terrestrial humic-like	**C2** Retelletti Brogi et al., 2020 **C2** Meng et al., 2013 **C1** Maie et al., 2014 **C2** Murphy et al., 2014a **C2** Lambert et al., 2016 **Peak α** Parlanti et al., 2000
C3	<250, 345	435	Fulvic-like	**C3** Retelletti Brogi et al., 2020 **C4** Lapierre and Del Giorgio, 2014 **C360/456** Stedmon et al., 2011 **C1** Maie et al., 2014 **C1** Lambert et al., 2016 **C3** Ferretto et al., 2017
C4	285	334	Protein-like	**C4** Retelletti Brogi et al., 2020 **C5** Murphy et al., 2006 **C3** Stedmon et al., 2011 **C3** Hur and Cho, 2012 **C3** Meng et al., 2013 **C5** Lambert et al., 2016 **C2** Ferretto et al., 2017 **Peak δ** Parlanti et al., 2000
C5	285	418	Fulvic-like	**C2** Chen et al., 2018 **C1** Lee et al., 2020 **C5** Stedmon and Markager, 2005 **C1** Yamashita et al., 2011 **C2** Murphy et al., 2006
C6	265	329	PAH-like	**C1** Gonnelli et al., 2016 **C3** Nie et al., 2016 **C6** Kothawala et al., 2014 **C3** Meng et al., 2013 **C7** Maie et al., 2014 **Peak δ** Parlanti et al., 2000

Chen, M., Jung, J., Lee, Y.K., Hur, J., 2018. Surface accumulation of low molecular weight dissolved organic matter in surface waters and horizontal off-shelf spreading of nutrients and humic-

like fluorescence in the Chukchi Sea of the Arctic Ocean. Sci. Total Environ. 639, 624–632. https://doi.org/10.1016/J.SCITOTENV.2018.05.205

Ferretto, N., Tedetti, M., Guigue, C., Mounier, S., Raimbault, P., Goutx, M., 2017. Spatio-temporal variability of fluorescent dissolved organic matter in the Rhône River delta and the Fos-Marseille marine area (NW Mediterranean Sea, France). Environ. Sci. Pollut. Res. 24, 4973–4989. https://doi.org/10.1007/s11356-016-8255-z

Gonnelli, M., Galletti, Y., Marchetti, E., Mercadante, L., Retelletti Brogi, S., Ribotti, A., Sorgente, R., Vestri, S., Santinelli, C., 2016. Dissolved organic matter dynamics in surface waters affected by oil spill pollution: Results from the Serious Game exercise. Deep. Res. Part II Top. Stud. Oceanogr. 133, 88–99. https://doi.org/10.1016/j.dsr2.2016.05.027

Hur, J., Cho, J., 2012. Prediction of BOD, COD, and total nitrogen concentrations in a typical urban river using a fluorescence excitation-emission matrix with PARAFAC and UV absorption indices. Sensors 12, 972–986. https://doi.org/10.3390/s120100972

Kothawala, D.N., Stedmon, C.A., Müller, R.A., Weyhenmeyer, G.A., Köhler, S.J., Tranvik, L.J., 2014. Controls of dissolved organic matter quality: Evidence from a large-scale boreal lake survey. Glob. Chang. Biol. 20, 1101–1114. https://doi.org/10.1111/gcb.12488

Lambert, T., Teodoru, C.R., Nyoni, F.C., Bouillon, S., Darchambeau, F.F., Massicotte, P., Borges, A. V., 2016. Along-stream transport and transformation of dissolved organic matter in a large tropical river. Biogeosciences 13, 2727–2741. https://doi.org/10.5194/bg-13-2727-2016

Lapierre, J.F., Del Giorgio, P.A., 2014. Partial coupling and differential regulation of biologically and photochemically labile dissolved organic carbon across boreal aquatic networks. Biogeosciences 11, 5969–5985. https://doi.org/10.5194/bg-11-5969-2014

Lee, S.-A., Kim, T.-H., Kim, G., 2020. Tracing terrestrial versus marine sources of dissolved organic carbon in a coastal bay using stable carbon isotopes. Biogeosciences 17, 135–144. https://doi.org/10.5194/bg-17-135-2020

Maie, N., Sekiguchi, S., Watanabe, A., Tsutsuki, K., Yamashita, Y., Melling, L., Cawley, K.M., Shima, E., Jaffé, R., 2014. Dissolved organic matter dynamics in the oligo/meso-haline zone of wetland-influenced coastal rivers. J. Sea Res. 91, 58–69. https://doi.org/10.1016/j.seares.2014.02.016

Meng, F., Huang, G., Yang, X., Li, Z., Li, J., Cao, J., Wang, Z., Sun, L., 2013. Identifying the sources and fate of anthropogenically impacted dissolved organic matter (DOM) in urbanized rivers. Water Res. 47, 5027–5039. https://doi.org/10.1016/j.watres.2013.05.043

Murphy, K.R., Bro, R., Stedmon, C.A., 2014a. Chemometric Analysis of Organic Matter Fluorescence, in: Aquatic Organic Matter Fluorescence. pp. 339–375.

Murphy, K.R., Hambly, A., Singh, S., Henderson, R.K., Baker, A., Stuetz, R., Khan, S.J., 2011. Organic matter fluorescence in municipal water recycling schemes: Toward a unified PARAFAC model. Environ. Sci. Technol. 45, 2909–16. https://doi.org/10.1021/es103015e

Murphy, K.R., Ruiz, G.M., Dunsmuir, W.T.M., Waite, T.D., 2006. Optimized parameters for fluorescence-based verification of ballast water exchange by ships. Environ. Sci. Technol. 40, 2357–2362. https://doi.org/10.1021/es0519381

Murphy, K.R., Stedmon, C.A., Wenig, P., Bro, R., 2014b. OpenFluor- an online spectral library of auto-fluorescence by organic compounds in the environment. Anal. Methods 6, 658–661. https://doi.org/10.1039/C3AY41935E

Nie, Z., Wu, X., Huang, H., Fang, X., Xu, C., Wu, J., Liang, X., Shi, J., 2016. Tracking fluorescent dissolved organic matter in multistage rivers using EEM-PARAFAC analysis: implications of the secondary tributary remediation for watershed management. Environ. Sci. Pollut. Res. 23, 8756–8769. https://doi.org/10.1007/s11356-016-6110-x

Parlanti, E., Worz, K., Geoffroy, L., Lamotte, M., Wörz, K., Geoffroy, L., Lamotte, M., 2000. Dissolved organic matter Fluorescence spectroscopy as a tool to estimate biological activity in a coastal zone submitted to anthropogenic inputs. Org. Geochem. 31, 1765–1781. https://doi.org/0146-6380/00/$

Retelletti Brogi, S., Balestra, C., Casotti, R., Cossarini, G., Galletti, Y., Gonnelli, M., Vestri, S., Santinelli, C., 2020. Time resolved data unveils the complex DOM dynamics in a Mediterranean river. Sci. Total Environ. https://doi.org/10.1016/j.scitotenv.2020.139212

Stedmon, C. a., Markager, S., 2005. Resolving the variability of dissolved organic matter fluorescence in a temperate estuary and its catchment using PARAFAC analysis. Limnol. Oceanogr. 50, 686–697. https://doi.org/10.4319/lo.2005.50.2.0686

Stedmon, C.A., Amon, R.M.W., Rinehart, A.J., Walker, S.A., 2011. The supply and characteristics of colored dissolved organic matter (CDOM) in the Arctic Ocean: Pan Arctic trends and differences. Mar. Chem. 124, 108–118. https://doi.org/10.1016/j.marchem.2010.12.007

Yamashita, Y., Kloeppel, B.D., Knoepp, J., Zausen, G.L., Jaffé, R., 2011. Effects of Watershed History on Dissolved Organic Matter Characteristics in Headwater Streams. Ecosystems. https://doi.org/10.1007/s10021-011-9469-z

Figure S8. (a) Total industrial activity in Tuscany from January 2005 to September 2020, the dashed line represents the average between 2005 and 2019, the standard deviation is indicated by the continuous lines. The inset shows a zoom of 2020 (January to September). (b) Tourist arrivals in Tuscany from 2012 to 2020. (c) Total movements (in or out) in the two major airports in Tuscany from 2014 to 2020 (data from 2019 were not available). (d) Land transportation movements between March and December 2020, from the Google community mobility report (categorized by movement purpose).

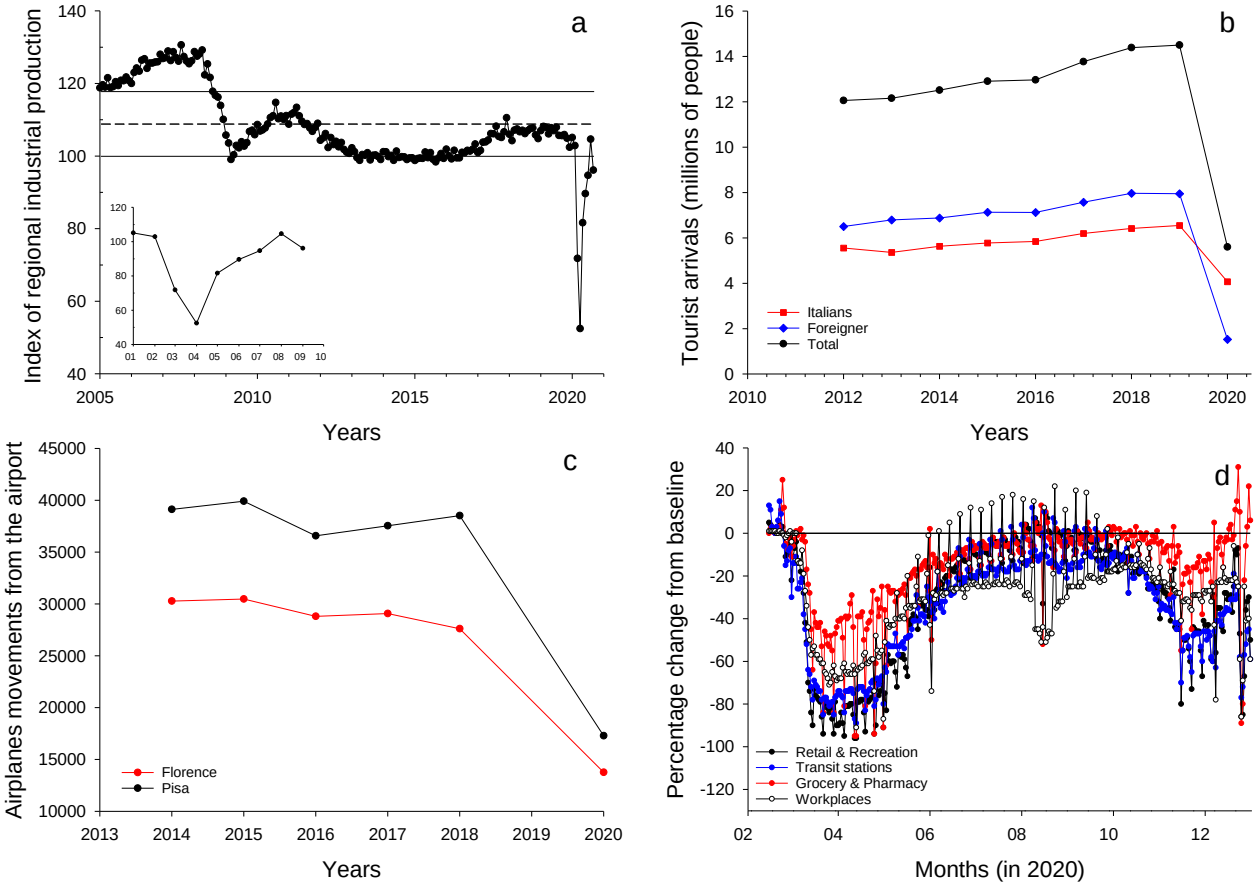

Table S2. Results of the stepwise regression. The sequence of inclusion (first column) of the variables (second column) in the regression model based on the marginal p-level (third column). Values of the coefficients and their standard error for the included variables (fourth and fifth column). Root Mean Square Error (RMSE) of the reconstructed DOC time series by the partial and final regression models (sixth column).

Steps	**Variables**	**min-max of the variable**	**p-values**	**coefficient of the model**	**Standard Error of the coefficient**	**RMSE of the model [μM]**
	Constant [μM]			239.8		
1	Runoff-90d *[m^3/s]*	0-400	$4.73 \cdot 10^{-09}$	-0.387	0.062	60.8
2	Lockdown period Mar-Jul 2020 [-]	0-1	$6.08 \cdot 10^{-22}$	-126.4	10.9	55.2
3	Temperature [°C]	5-32	$7.63 \cdot 10^{-16}$	7.268	0.795	45.5
4	Runoff-2d *[m^3/s]*	0-1000	$3.10 \cdot 10^{-07}$	0.160	0.030	42.9
5	Lockdown period Aug-Nov 2020 [-]	0-1	$3.12 \cdot 10^{-04}$	-34.5	9.3	40.8
6	Runoff-30d *[m^3/s]*	0-600	$8.80 \cdot 10^{-03}$	-0.176	0.066	39.7
7	HPA *[cells/ml]*	0-1E7	$2.57 \cdot 10^{-03}$	$-6.7 \cdot 10^{-06}$	$2.2 \cdot 10^{-06}$	38.8
Not included in the model	runoff-1d [m3/s]	0-1000	$3.29 \cdot 10^{-01}$			
	Lockdown period Mar-May 2020 [-]	0-1	1.00			
	Lockdown period Mar-June 2020 [-]	0-1	$3.48 \cdot 10^{-01}$			
	Lockdown period Mar-Aug 2020 [-]	0-1	$4.87 \cdot 10^{-01}$			
	Lockdown period Jul-Oct 2020 [-]	0-1	$5.05 \cdot 10^{-01}$			
	Lockdown period Jul-Dec 2020 [-]	0-1	$2.79 \cdot 10^{-01}$			
	Lockdown period Jul2020-Jan2021 [-]	0-1	$3.59 \cdot 10^{-01}$			
	Lockdown period Jun-Oct 2020 [-]	0-1	$5.05 \cdot 10^{-01}$			
	Lockdown period Jul-Nov2020 [-]	0-1	$8.40 \cdot 10^{-01}$			
	Lockdown period May-Nov 2020 [-]	0-1	$2.59 \cdot 10^{-01}$			
	runoff-3d [m3/s]	0-1000	$8.36 \cdot 10^{-01}$			
	runoff-60d [m3/s]	0-300	$5.44 \cdot 10^{-01}$			
	runoff-120d [m3/s]	0-200	$5.44 \cdot 10^{-01}$			

Figure S9. Arno River absorption coefficient at 254 nm (a_{254}) in 2014, 2015, 2020, and 2021, error bars represent the standard deviation (n=3).

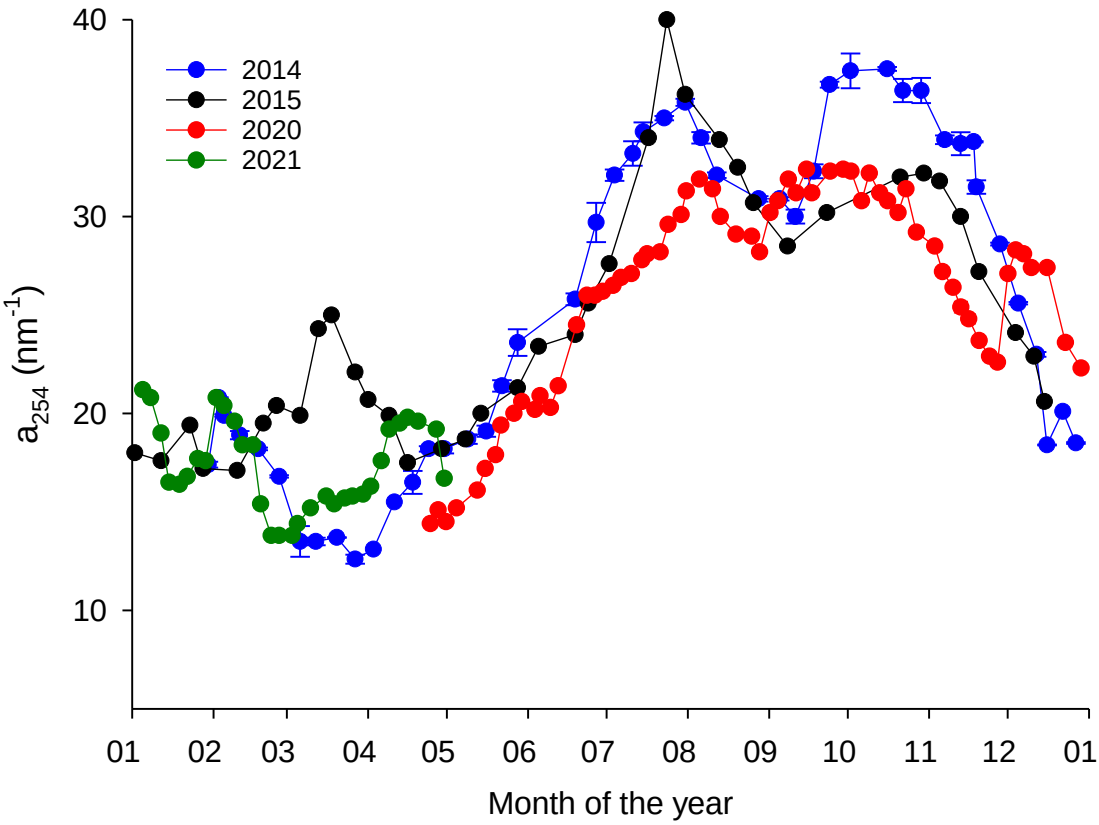

Figure S10. Annual trend of the 6 components identified by PARAFAC analysis of the EEMs in 2014, 2015, 2020, and 2021, error bars represent the standard deviation (n=3).

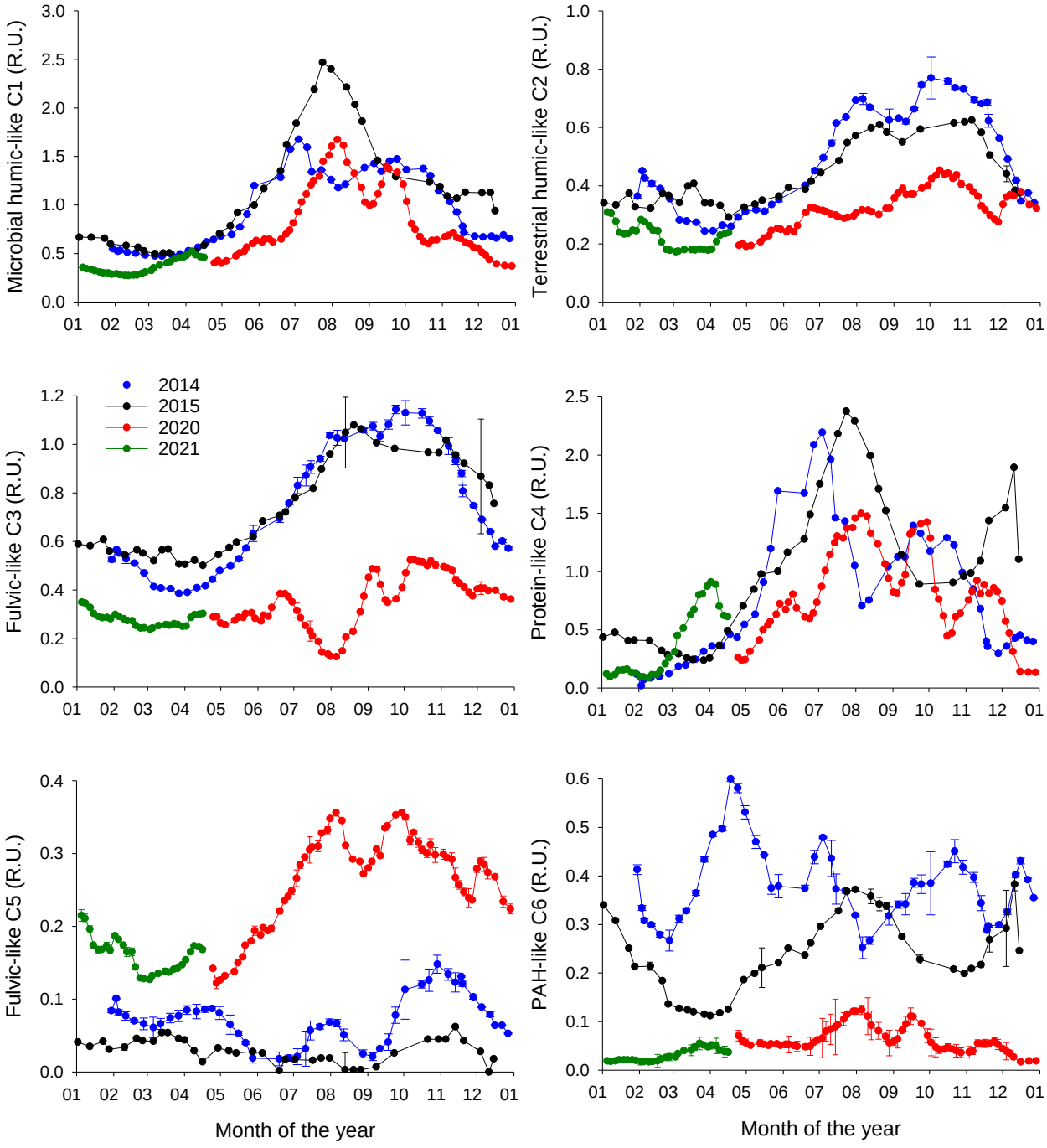

Figure S11. Annual trend of high nucleic acid heterotrophic prokaryotes (HP), shown as a percentage of the total HP.

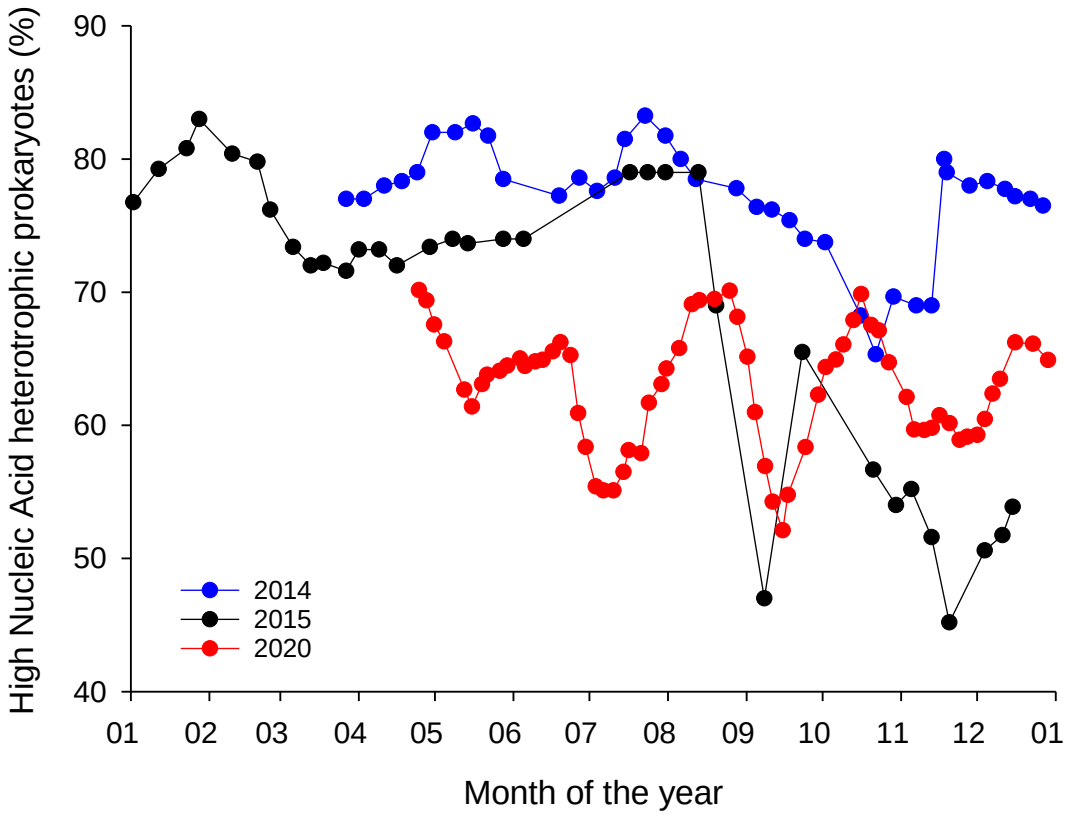

Figure S12. Distribution of dissolved organic carbon (DOC) in the coastal area in front of the Arno River estuary on May 5th, 2020.

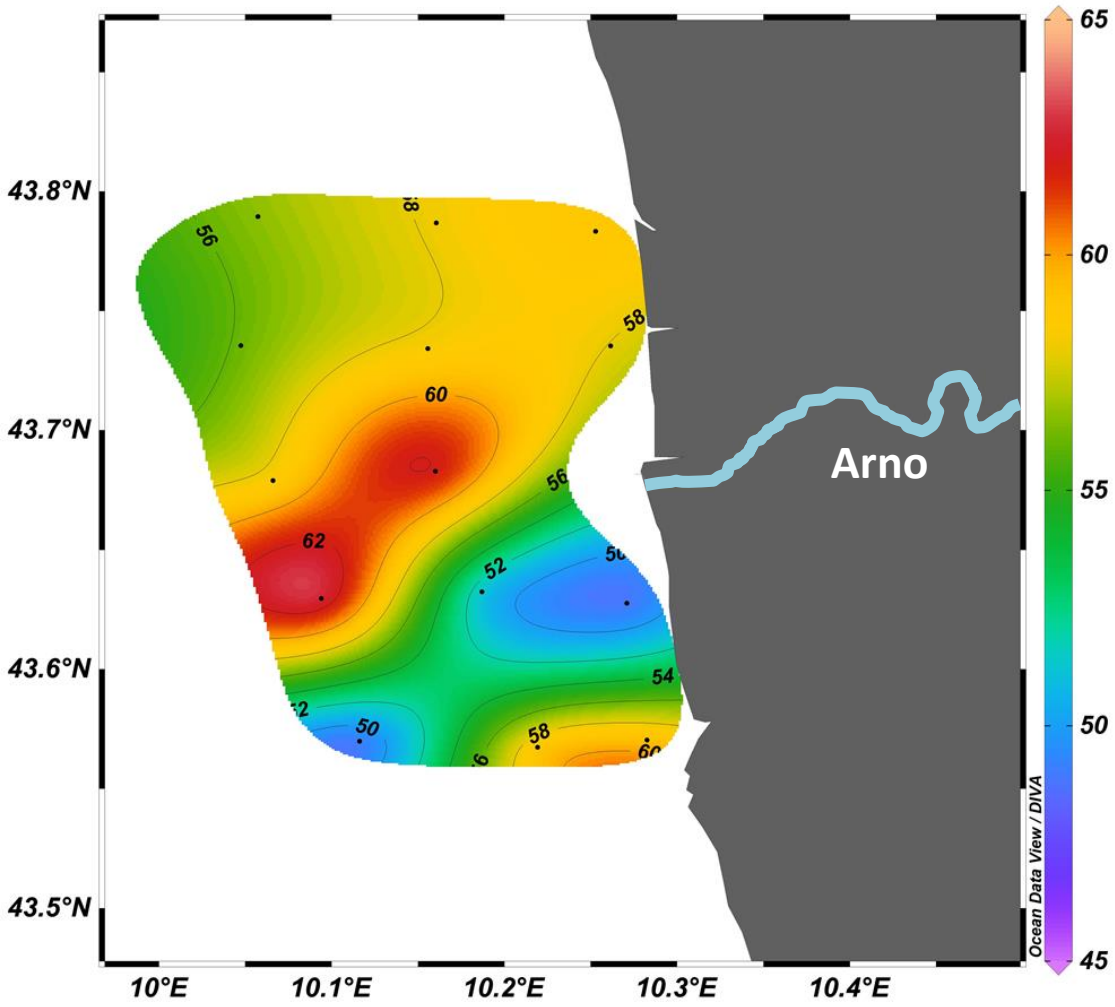

Figure S13. Comparison of monthly means of air temperature (a), precipitation (b), and discharge (c) between 2020 (dark line) and the climatology (colored lines and shaded areas). Light-colored areas represent the 05th and 95th percentile, dark-colored areas represent the 25th and 75th percentile.

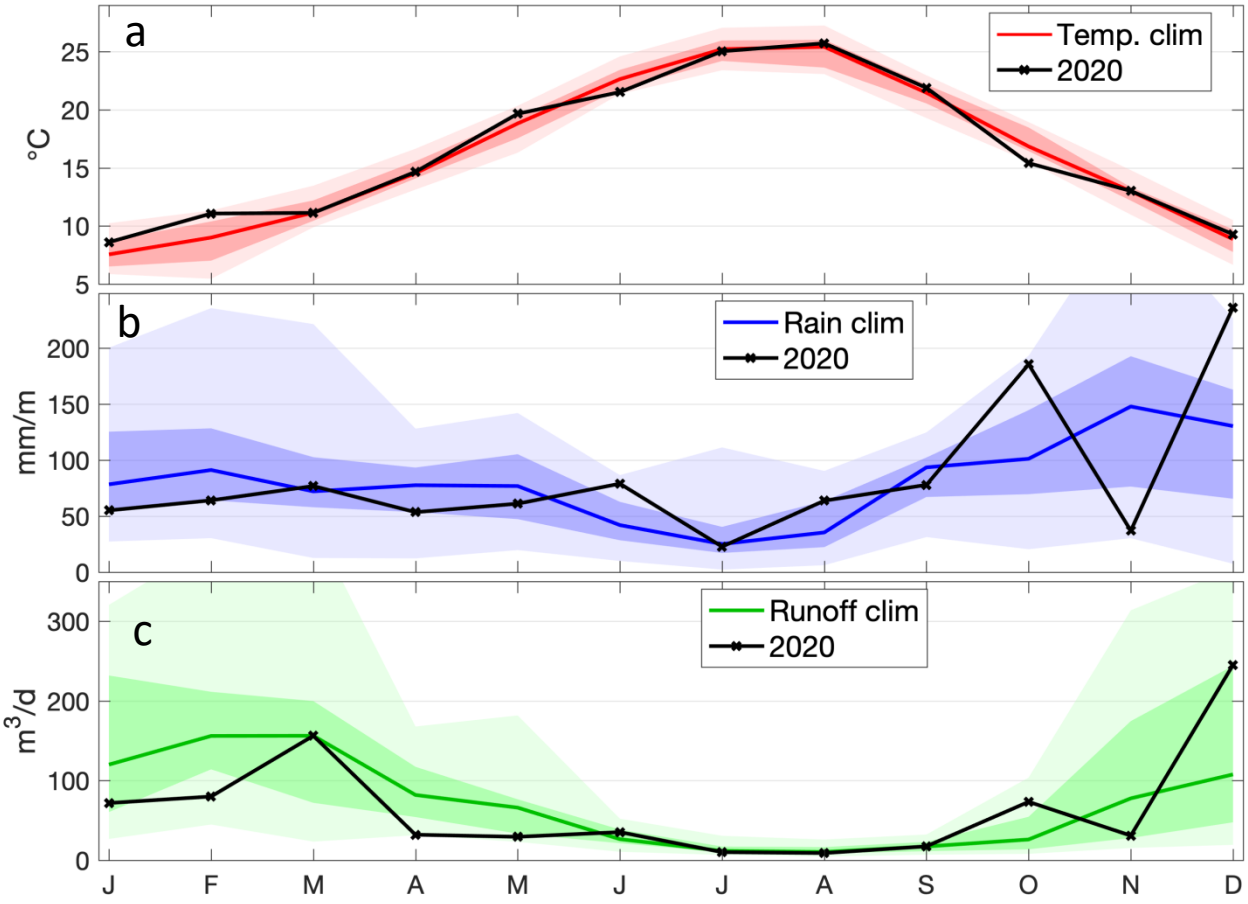

Figure S14. River surface water temperature in 2014, 2015, 2020 and 2021